SENSITIVITY IMPROVEMENT OF WIRELESS PRESSURE SENSOR BY INCORPORATING A SAW REFLECTIVE DELAY LINE

Haekwan Oh, Weng Wang, Keekeun Lee, Ikmo Park, and Sang Sik Yang*

Division of Electronics Engineering

Ajou University, Suwon, S. Korea, 443-749

*Email: ssyang@ajou.ac.kr

Abstract - this paper presents a wireless surface acoustic wave (SAW) pressure sensor on 41°YX $LiNbO_3$ for tire pressure monitoring system (TPMS) application, in which a reflective delay line composed of an interdigital transducer (IDT) and several reflectors was used as the sensor element. Using the coupling of modes (COM), the SAW reflective delay line was simulated, and the optimal design parameters were determined. The fabricated 2.4GHz SAW sensor was wirelessly characterized by the network analyzer. Sharp reflection peaks, few spurious signals, and relatively high signal-to-noise (S/N) ratio were observed. High sensitivity of 2.9 deg/kPa and good linearity were observed.

Index terms: coupling of modes, interdigital transducer, $LiNbO_3$, piezoelectric substrate, reflective delay line, surface acoustic wave, wireless pressure sensor, temperature compensation

I. INTRODUCTION

Recently, surface acoustic wave (SAW) pressure sensors have gained an increasing amount of attention for wireless tire pressure monitoring systems (TPMSs), owing to their high sensitivity, small size, low cost, easy reproducibility, and good stability [1-2]. Typical SAW based pressure sensors are composed of two resonators. One is placed in the sensing area (in the center of the diaphragm) and the other is used as a reference sensor to compensate the temperature effect (depending on its location on the substrate). A differential frequency output

resulting in the phase shifts of the reflected peaks depending on the applied pressure value. By evaluating the phase shifts, we can extract the external pressure values.

To find the optimal design parameters, the coupling of modes (COM) modeling and finite element methods (FEMs) were performed. The device was fabricated according to the extracted design parameters and then wirelessly characterized using an RF network analyzer. In this paper, we describe the process used to create reliable SAW sensor structures, their electrical and mechanical performance, and a comparison between the simulated and measured results.

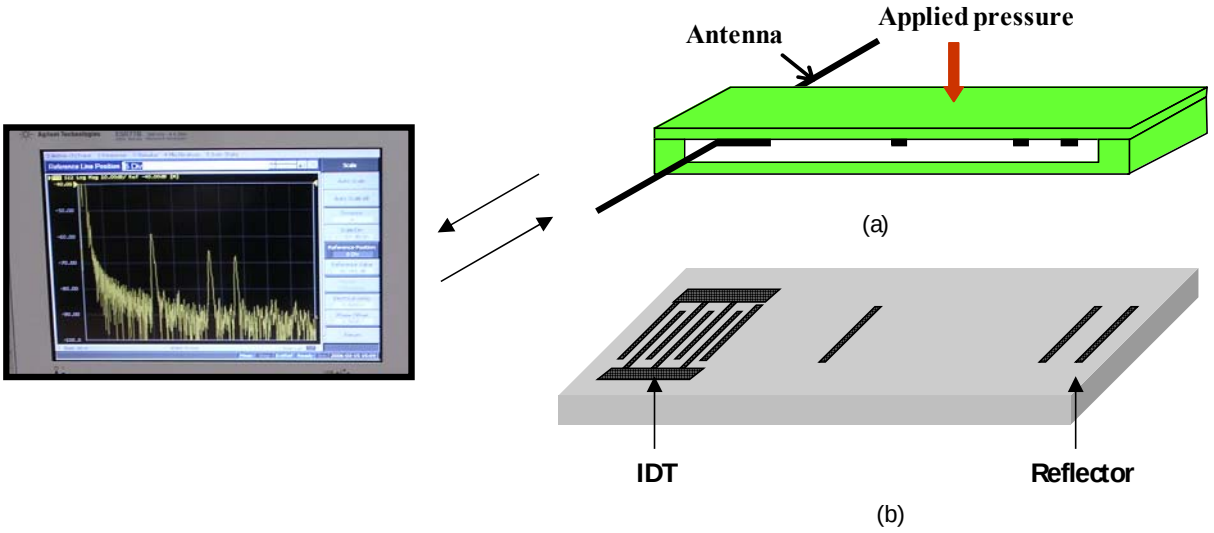

Figure 1. Schematic diagram of the SAW pressure sensor system. (a) 3-dimensional view of the SAW pressure sensor and (b) flip-over view of the top diaphragm.

II. THEORETICAL ANALYSIS OF SENSOR RESPONSE MECHANISM

A mechanical analysis of SAW propagation on the pre-stressed piezoelectric diaphragm was studied using FEM stress analysis [8]. The basic structure of the pressure sensor and coordinate system are shown in Figure 2. The sensor is composed of a piezoelectric diaphragm (example of 41° YX $LiNbO_3$) and a sensor cover. The SAW propagates along the x_1 axis on the x_1-x_2 plane at x_3=0. For the analysis, all of the material parameters of the medium are transformed into this coordinate system. Using the wave motion equations and electrical boundary conditions at x_3=0, a set of equations for the stress T *and* electric displacement D, the SAW displacement U and the electrical potential φ are given by Eq. (1).

following,

$$\begin{bmatrix} C_{66}+C_{44}a^2-\rho v^2 & e_{16}+e_{34}a^2 \\ -(e_{16}+e_{34}a^2) & \varepsilon_{11}+\varepsilon_{33}a^2 \end{bmatrix} = 0. \qquad (4)$$

Eq. (4) is an algebraic equation of the fourth order in α so that for a given value of the SAW velocity v we obtain two eigenvalues of α with a negative imaginary part. For both eigenvalues of α, the eigenvectors β_1 and β_2 of the normalized amplitudes of Eq. (1) vanish at infinity from Eq. (3). Then U_2 and φ are represented as

$$\begin{cases} U_2 = \sum_{n=1}^{2} A_n \beta_{1n} \exp(-\alpha_n k x_3) \times \exp(i\omega t - ikx_1) \\ \varphi = \sum_{n=1}^{2} A_n \beta_{2n} \exp(-\alpha_n k x_3) \times \exp(i\omega t - ikx_1) \end{cases}, \qquad (5)$$

with A_n as the normalized amplitudes.

For the full description of the SAW, the electric potential φ, the electric displacement along the x_3 direction D_3 and the stress T_{3i} (i=1,2) must satisfy the boundary continuity conditions at x_3=0. The mechanical stress continuity conditions are described by Eq. (6).

$$\begin{aligned} T_{31}|_{x_3=0} &= T_x \\ T_{32}|_{x_3=0} &= T_y \end{aligned}, \qquad (6)$$

where T_x and T_y are the applied stress components which are calculated by FEM analysis. The electric displacement continuity boundary conditions are described by Eq. (7).

$$\begin{cases} D_3 = e_{3kl}\partial U_k/\partial x_l - \varepsilon_{ik}\partial\varphi/\partial x_k \text{ (for } x_3>0) \\ D_{30} = -\varepsilon_0 \partial\varphi'/\partial x_3 \text{ (for } x_3<0),\ \varphi' = \varphi|_{x_3=0} \times \exp(kx_3) \\ D_3|_{x_3=0} = D_{30}|_{x_3=0} \end{cases} \qquad (7)$$

where ε_0 is the vacuum dielectric constant. The substitution of the general solution, Eq. (5), into the boundary conditions leads to a second set of homogeneous linear equations forming the normalized amplitudes β_1 and β_2. A nontrivial solution again requires that the determination vanishes at an assumed velocity value, i.e.,

whereas it is faster in the compressed section. Φ_i (i=1,2,3) are the relative phase changes of the i^{th} reflector (R_1, R_2 and R_3 in Figure 4).

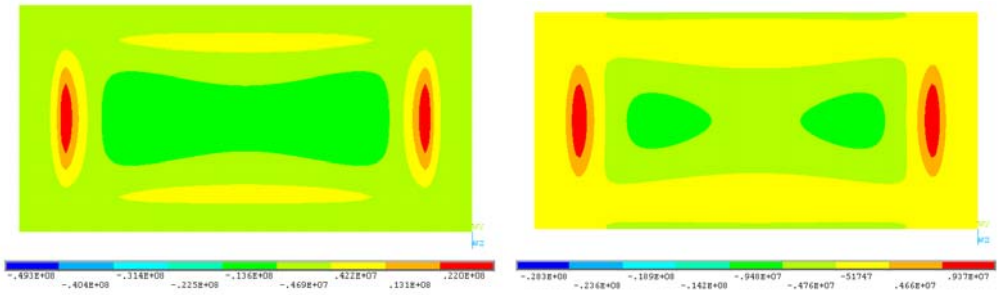

Figure 3. Calculated stress distribution on $LiNbO_3$ diaphragm under 300kPa pressure in cases of (a) 350μm thick diaphragm and (b) 500μm thick diaphragm.

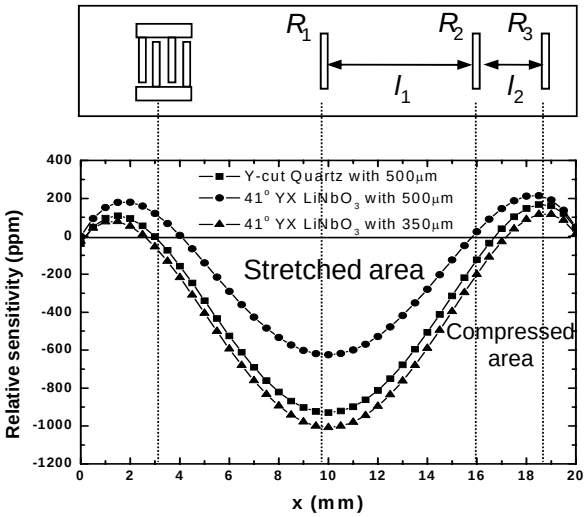

Figure 4. Relative phase changes along the SAW propagation path in case of Y cut quartz and 41° YX $LiNbO_3$ under 300kPa pressure.

Also, Figure 4 shows that varying the diaphragm thickness results in the variation of the diaphragm bending, strain/stress distribution, and corresponding velocity change. The effect of the piezoelectric diaphragm thickness on the sensitivity of the sensor (calculated from Eq. (10)) was evaluated and shown in Figure 5, in which the simulation parameters are as follows: 41° YX $LiNbO_3$ substrate, operation frequency substrate of 2.4GHz and diaphragm area of 8 mm×4 mm. The thickness was varied from 150μm to 400μm. Figure 5 shows the calculated phase shift of the sensor with respect to the diaphragm thickness under a pressure of 200kPa.